

Key words: *axial compressor stage, unsteady flow, Inlet Guide Vane-Rotor interaction*

ANDRZEJ WITKOWSKI, MIROSLAW MAJKUT***

EXPERIMENTAL INVESTIGATION OF INLET GUIDE VANE-ROTOR INTERACTION IN A LOW SPEED AXIAL FLOW COMPRESSOR STAGE

The two dimensional steady and unsteady flow field at midspan in a low speed axial flow compressor stage has been investigated experimentally, using two systems, based on totally different principles: a 2-sensor fast response straight and 90° triple split fiber probes (TSFP) and two dimensional LDA system with an emphasis on the interaction of the inlet guide vane (IGV) wake with the rotor flow field. To account for the uniformity of the rotor absolute inlet flow field, measurements has been made at eight tangential locations in the absolute frame equally spaced over one IGV pitch. The time resolved investigation, done by TSFP and LDA allows to presenting velocity fields, flow angles and turbulence data at different IGV-rotor positions during one blade passing period. The velocity measurements are decomposed into a time averaged velocity, a periodic velocity component and a unresolved velocity component. Using two measurement systems, one being intrusive and the other non-intrusive, in the same complex flow field, gives the opportunity for a critical comparison of results and opens the view for further improvements. Averaging these results, enabled also comparison with the pneumatic five-hole probe measurement.

1. Introduction

The flow in axial flow compressor stage is not only highly three dimensional, but also features complex unsteady phenomena. One of the major sources of unsteadiness is the aerodynamic interaction between inlet guide vane and rotor. One aspect of rotor stator interaction is caused by the wakes generated by the airfoils upstream of a blade row. The wakes strongly influence the inlet flow at the next blade row resulting in periodic total pressure

* *Silesian University of Technology, 44-100 Gliwice, Konarskiego 18 Str.,
E-mail: andrzej.witkowski@polsl.pl*

** *Silesian University of Technology, 44-100 Gliwice, Konarskiego 18 Str.,
E-mail: miroslaw.majkut@polsl.pl*

fluctuations and periodic variations of incidence angle. Especially during operations of compressors with variable inlet guide-vanes in situations with high setting angles of the guide-vanes, the interaction can be suppressed so heavily that rotating disturbances can exist. Although there has been extensive theoretical and experimental research done on compressor rotor wakes, not much work has been done on influence of IGV wakes at different stagger angle on the following rotor blade row. Many researches have investigated rotor-stator interaction. Poensgen et al. [1], [2], Zaccaria and Lakshminarayana [3], [4], Freudenreich and Fransson [5], Sharma et al. [6], Reinhold and Bohne [7] provide comprehensive surveys of unsteady flow in turbomachinery. The experimental unsteady flow investigation were also accompanied and aided by numerical calculations, Kazimierski [8], and Arnone et al., [9], [10]. Unfortunately most of these investigations have been done on isolated airfoils, highly loaded axial compressors or axial turbines and not much work has been done on the influence of stagger angle of IGV on the unsteady flow field in the axial flow low speed compressor stage. Although all aspects of this interaction are not fully understood nowadays, it is well-known that by properly indexing stator vanes and rotor blades, the efficiency of a multistage turbomachinery component can be altered and improved, see e.g. Nichuis et al. [11].

On the other hand, the data can be used for a comparison with the results of advanced numerical flow calculations, which are capable of performing full-stage calculations by coupling the grids of inlet guide stator vanes and moving rotor blades [12].

2. Experimental facility and instrumentation

2.1. Experimental facility

The experiments has been performed in the axial flow low speed compressor stage (AFLSCS) of the Institute of Power Engineering and Turbomachinery at the Technical University in Gliwice, which was designed to tests compressor stages over a wide range of parameters and to validate numerical codes. It consists of an inlet guide vane followed by a rotor with a hub to tip annulus wall diameter ratio 0.56, with outer diameter of 1.0 m, with 16 cambered and twisted blades of British C-4 section, designed for free vortex operation, followed by a 13-vane stator row and the outflow curvilinear diffuser with the throttling blades (Fig. 1).

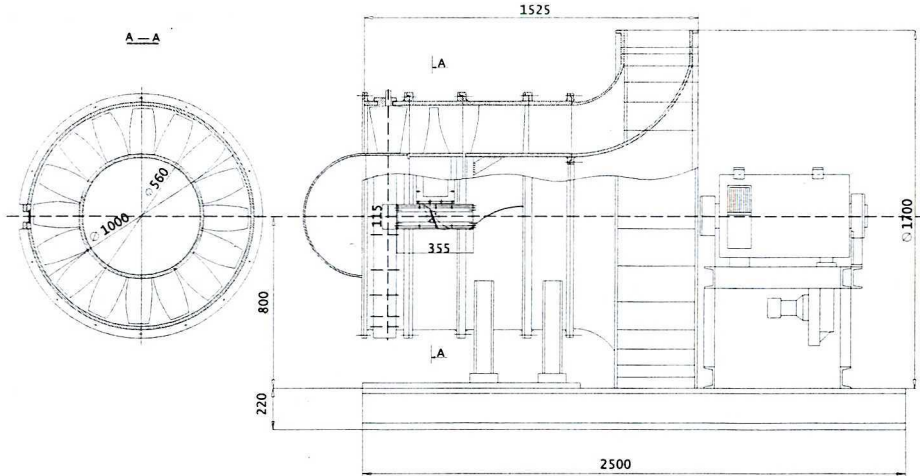


Fig. 1. Axial flow low speed compressor stage

Table 1.

Rotor blade row geometry and operating characteristics

Rotor blade chord (at midspan)	0.13 m
Rotor pitch/chord ratio (at midspan)	1.17
IGV-rotor spacing normalized by rotor axial chord (at midspan)	1.58
Rotor-stator blade row spacing normalized by rotor axial chord (at midspan)	1.71
Pressure rise coefficient ψ_N	0.365
Flow coefficient φ_N	0.374
Rotor inlet Mach number Ma_{1r}	0.12

Table 1 lists the overall design point parameters along with some referent dimensions. The compressor stage can be operated with variable stagger angles of the IGV, which can be set individually. To account for the uniformity of the rotor absolute inlet flow field, special mechanisms were designed to allow the IGV to be moved circumferentially relative to the stationary probes. The research compressor stage is connected to the suction side of the measuring collector and consists of the large bellmouth inlet for mass flow measurement. The facility is terminated downstream by an aerodynamically designed throttle, which provides control of a stage operating characteristics. The details of the design of the facility, their performance and geometrical features are described by Witkowski et al. [13], [14]. The pressure rise and efficiency characteristic at different IGV setting angles as well as the mea-

suring points, selected for further detailed flow investigation, are shown in Fig. 2.

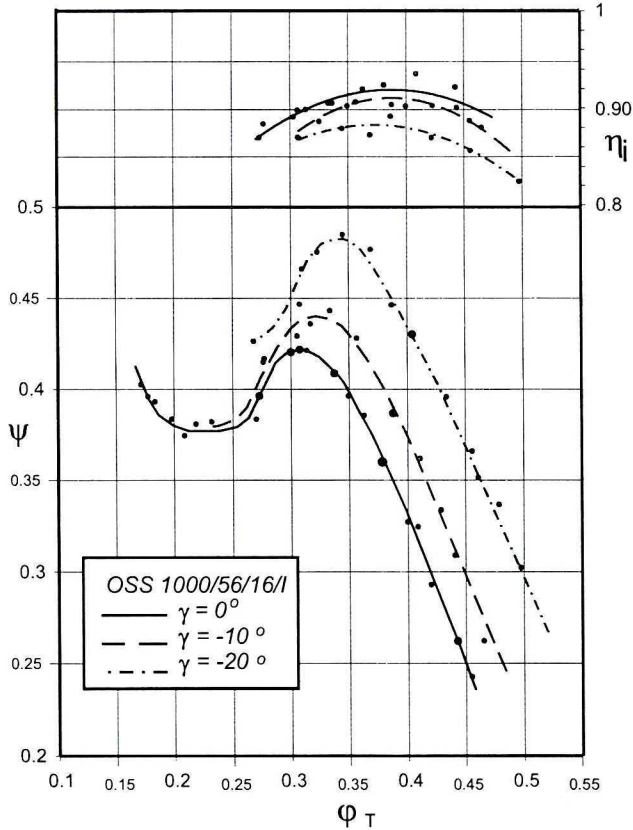


Fig. 2. Overall performance characteristics of the rotor

Through proper use of LDA and TSFP the entire steady and unsteady flow field, including the wall layers, can be measured in the compressor stage. For the present tests a flat quartz glass window (quality: BK 7) covering the entire flow field from upstream to downstream of the rotor passage, is inserted in the casing, to provide optical access for laser anemometry. This plane parallel 3 mm thick window has an axial extension 344 mm and 45 mm extension in circumferential direction. A 0.51 mm step exists between the plane parallel window and the curved casing. No detectable influence on the flow was found at positions $>10\%$ flow channel height behind the window, Giess and Kost [15]. The rotor endwalls were painted with a high-temperature black paint to reduce surface reflections. A completely automated data processing system is built around a PC computer.

2.2. Triple-split fiber probe (TSFP) anemometer system

The unsteady two-dimensional flow field upstream and downstream of the rotor has been sampled periodically using straight triple split fiber probe (TSFP). The probe consists of a cylindrical quartz-fiber of a diameter of 400 μm divided into three parallel sensor paths. The frequency response of that probe is up to 175 kHz. The probe has been tested in a free laminar jet in the velocity ranges 2–50 m/s [12]. The calibration procedure, which requires 135 combinations of the flow and angle, is performed semi-automatically by a computer connected to the measuring system. It appears that the magnitude of the velocity vector can be measured with an accuracy of $\pm 3\%$, while the flow angle can be measured with a standard deviation less than $\pm 0.5^\circ$. Statistical errors result from a finite number of measured events. In our case of performed measurements, a minimum number of successfully evaluated time events of 1000 was achieved at every measured points in the wake close to the rotor trailing edge. All statistical errors are given for 95% confidence interval. The unsteady 2D-TSFP data acquisition was triggered by an once-per-blade signal. One rotor pitch was subdivided into 50 equally spaced increments, describing the special resolution in the rotor relative coordinate system. The periodic influence from upstream IGV onto the unsteady rotor flow was taken into account by subdividing the traverse of one IGV passage into 8 steps. At each of the 50 points covering the rotor pitch, the time-average 2D velocity vector in the rotor relative frame was calculated. A more detailed description of the measuring system, TSFP and their calibration procedure is given in [12] and [16].

2.2. Laser-Doppler anemometer (LDA) system

The LDA system used is a three-color, six-beam, three-dimensional measuring system. It consists of a 4 W argon-ion laser, tuned to the 476.5 nm (violet), 488 nm (blue) and 514.5 nm (green lines), a transmitter, six manipulators, a two 60 mm 1D and 2D laser probes, three photomultipliers, color separator, and interference filters, and external data interface with rotating machinery encoder for tagging LDA bursts with the angular rotor position, a three axis traversing system with control unit, a 650 MHz Pentium II DELL PC for data acquisition, reduction and visualization. The focal length of LDA probes is 160 mm or 400 mm with additional lenses producing a beam intersection diameter 78 μm or 194 μm and an intersection lengths of about 0.66 mm or 4.09 mm, respectively. The green, violet and blue pairs are used to measure the axial, tangential and radial components of velocity respectively. The fringe spacing are 2.18 μm ($\lambda = 514.5 \text{ nm}$), 2.07 μm ($\lambda = 488 \text{ nm}$) and 2.02 μm ($\lambda = 476.5 \text{ nm}$). The probes are mounted on a

supports attached to a mechanical traverse. The traverse can move axially, horizontally and vertically, and can be turned in horizontal plane to achieve the measurement at the desired location in the compressor stage. The three linear degrees of freedom plus turn make it possible to position the probe very accurately (± 0.125 mm). The LDA unit is remotely placed and connected by long (15 m) optical fibers to the compressor rig. The entire system comprising the laser, the transmitting and receiving optics is mounted on an optical bench for easy alignment. The LDA system is free to acquire velocity measurements whenever a seed particle crosses the LDA probe volume. In the rotor flow field, this results in the random acquisition of many velocity measurements during every rotor revolution. To obtain strong enough light impulses for the LDA, particles with mean diameter of 0.6–1.0 micrometer must be used. The seeding to be used for investigation is silicon oil and this enters the compressor stage from a nozzle situated upstream of the inlet. The oil is atomized by a Safex Fog Generator 2010. In the LDA measurements, the measuring system as it was used for TSFP, has been adapted (Fig. 3).

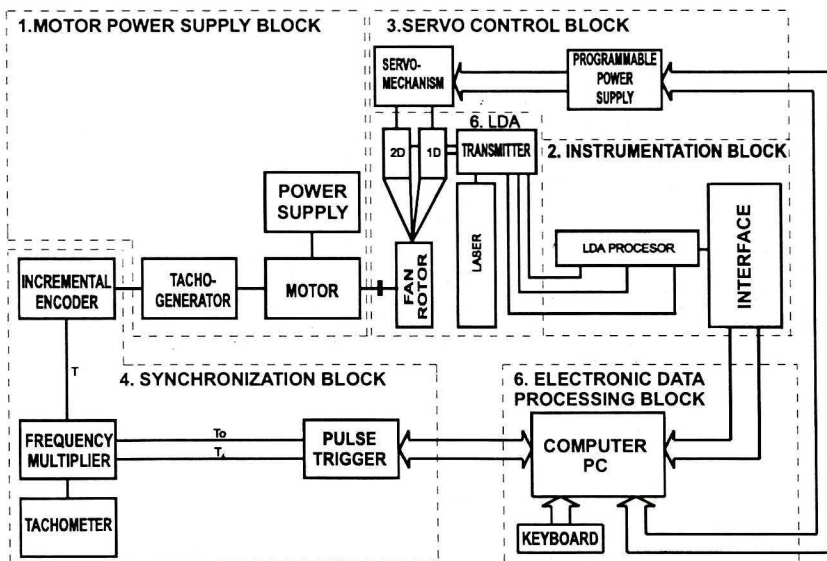


Fig. 3. Schematic set up diagram of the LDA measuring system

Thus to relate a measurement event to the rotor position, an optical shaft encoder has been attached to the compressor shaft. This encoder divides one revolution of the rotor into 3600 counts and since there are 16 rotor blades, this comes to 225 counts per rotor passage. One rotor passage is then divided into 50 measurement windows, each of which has 4.5 counts and is 3.063 mm length at midspan. Each velocity measurements is tagged with the angular

Measurements has been acquired at 101 axial measurement locations from just upstream of the rotor (0.735 chord) to one axial chord downstream of the rotor midspan. In order to get the spanwise characteristics of the unsteady flow, the measurements has been carried out at 38 radius, 44 percent of the axial chord of the rotor downstream of the rotating blade. Since only a straight TSFP and two-dimensional LDA was used for measurements, only the velocities in the axial and tangential directions are measured. To account for the uniformity of the rotor absolute inlet flow field, measurements has been made at eight tangential locations in the absolute frame equally spaced over one inlet guide vane (IGV) pitch (as shown in Fig. 4). There are several criteria that can be used to identify the effect of the IGV wake on the flow field in the rotor blade wake. Compared to the free-stream and wake flow downstream of the rotor without influence of the IGV wake, the rotor blade wake has a higher velocity defect, higher unresolved unsteadiness, a variation in flow angle across the IGV wake, and higher shear stress in the presence of the IGV wake. These criteria will be used in this section to determine the presence and interaction between the IGV wake and the rotor blade wake. An indication of the level of interaction between the IGV and rotor flow field can be assessed by examining the ratio of the time it takes the rotor to traverse one IGV pitch versus the time it takes for fluid particles to travel through the rotor blade passage. This is called the reduced frequency and it is given by

$$\Omega = \frac{l_z}{W_z} \left/ \frac{S_{IGV}}{U_m} \right. \quad (1)$$

where: Ω is the reduced frequency, l_z is the rotor axial chord, W_z is the axial velocity at the inlet to the rotor, and S_{IGV} is the IGV pitch.

This ratio determines the number of IGV wakes in each rotor passage at any instant time. For the compressor stage in this investigation, the spanwise distribution of the reduced frequency at different stagger angle of IGV is shown in Fig. 5. At midspan the reduced frequency is 0.75, which means that there should be not complete IGV wake in each rotor passage for each IGV/rotor blade location, which is demonstrated in the following paragraphs.

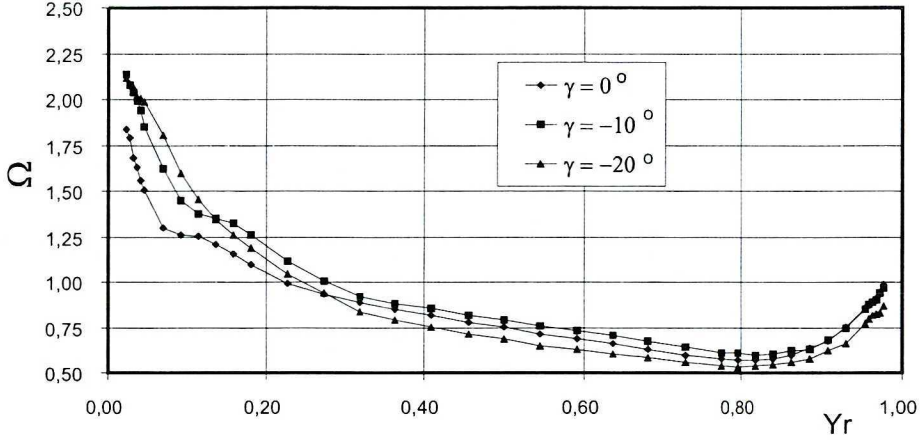


Fig. 5. Spanwise distribution of the reduced frequency

2.4.2. Data processing

For the TSFP/LDA measurements downstream of the rotor, the instantaneous velocity is decomposed as follows

$$C = \bar{C} + \tilde{C} + C' \quad (2)$$

where $\bar{C} = \frac{1}{MN} \sum_i^M \sum_n^N C_{i,n}$ is time averaged velocity, $C' = \tilde{C} - \bar{C}$ is periodic

velocity component, $\tilde{C} = \frac{1}{N} \sum_{i=1}^N C_{i,n}$ is the periodic unsteady velocity which results from relative motion of the rotor with respect to the following stator vane and $C' = C - \tilde{C}$ is the unresolved unsteady velocity which is any flow fluctuation that is not correlated with the rotor speed. From this velocity decomposition, the axial unresolved unsteadiness can be computed:

$$T_{zi} = \frac{\sqrt{\bar{C}'^2_{zi}}}{\tilde{C}_i} \quad (3)$$

where: $\bar{C}'^2_{z,i} = \frac{1}{N} \sum_{n=1}^N (C_{z,i,n} - \tilde{C}_{z,i})^2$.

3. Experimental results

3.1. Inlet guide vane-rotor blade row spacing

Fig. 6 shows contour plots of absolute velocities and axial components of unresolved unsteadiness distribution in the IGV-Rotor blade row spacing at IGV setting angles $\gamma = 0^\circ$ to understand the propagation of the IGV wake through IGV-rotor blade row spacing. LDA measurements were taken at midspan only, where the flow is expected to be most two-dimensional.

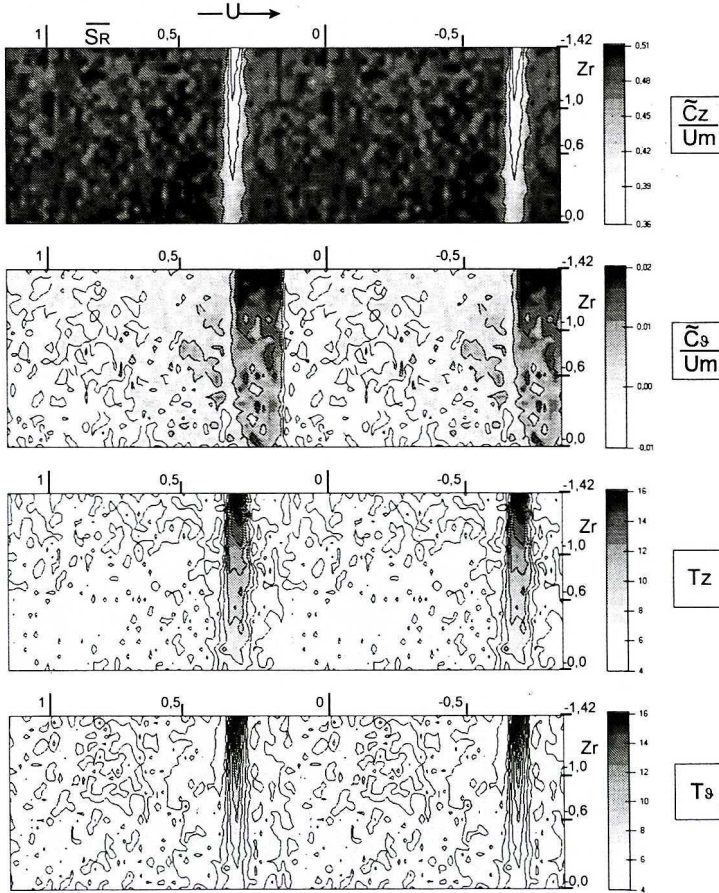


Fig. 6. Contour plots of IGV wakes in the IGV-rotor passage: $\gamma = 0^\circ$, $\varphi_T = 0.374$, $Y_r = 0.5$

A knowledge of the rate of decay for the IGV wake defect and unresolved unsteadiness is necessary for understanding of the IGV-rotor interaction. In the following figure (Fig. 7), the result at traverse depth positions ($Z_r = -1.3$; 1.0 and -0.6) were plotted to exhibit the decay characteristics of the IGV

wake with streamwise distance. While the wake velocity defect and maximum unresolved unsteadiness are very high in the trailing edge region, they decay rapidly as the wake travels downstream.

The comparison of the circumferential distribution of the axial component of absolute velocities in the IGV wakes normalized by the mean rotor speed (Fig. 8a) and by the mean velocity \bar{C}_z , determined by the use of TSFP and LDA with results determined by FHP (Fig. 8b) shows reasonable agreement in the vicinities of the center blade wake.

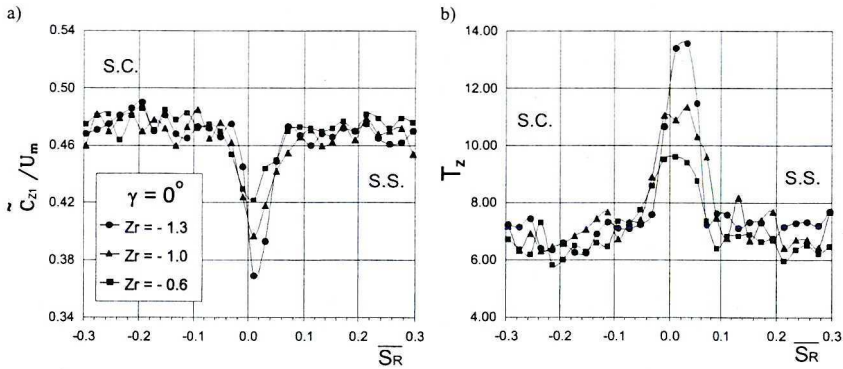


Fig. 7. Decay of IGV wake velocity defect (a) and unresolved unsteadiness (b) with streamwise distance: $\gamma = 0^\circ$, $\varphi_T = 0.374$, $Y_r = 0.5$

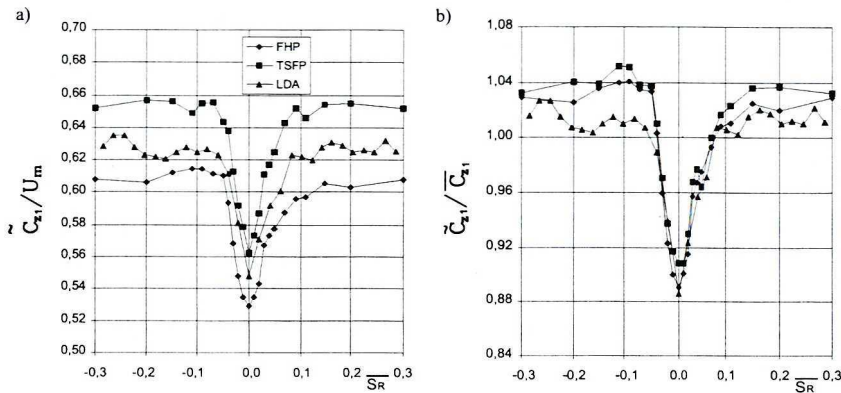


Fig. 8. Comparison of IGV wake velocity profiles, normalized by U_m (a) and \bar{C} (b), determined by the use of FHP, TSFP and LDA at $Z_r = -0.8$, $\gamma = 0^\circ$, $\varphi_T = 0.374$

In the free stream region, where velocity component could differ by as much as 6.3% and 3.5% respectively, the agreement is not so satisfactory. However, the agreement is significantly better as the velocities are normalized by mean velocity \bar{C}_z .

3.2. Rotor passage flow field

3.2.1. Relative velocity distribution

The contour plots of the ensemble average relative velocity normalized by mean rotor speed (U_m) at eight different IGV/rotor locations is presented in Fig. 9. Since these eight different locations are equally spaced over one IGV pitch, they can be viewed sequentially from IGV/rotor location one to location eight and then back to one again. The regions near the stagnation point and near the pressure and suction side as well close to the trailing edge of the rotor blades could not be investigated with the LDA. This region contains the area of the blade, and the blade shadow that can not be penetrated by the laser beams. More a lack of tracer particles occurs in region filled with boundary layer fluid, as wakes and strong secondary vortex regions.

Figure 9 shows the flow deceleration through the blade passage. The velocity decelerates significantly on the suction side from the leading edge to $Z_r = 0.9$ after all it levels off and becomes fairly uniform, up to the trailing edge. This generates unsteady forces on the blade, which can excite blade vibration and may cause high cycle fatigue problems, hence compromising the life of the blade. Therefore, it is very important for compressor designers both to understand the origin of such unsteady forces and to develop the capability to accurately simulate them in order to be able to predict its effect on the blade vibration and eventually to be able to propose design changes to diminish such effects. Measuring the flow inside the rotor blades with a LDA, they showed that there are two distinct flow fields, which can be called the minimum and maximum interaction between the IGV wake and the main blade to blade flow. Examining the position 4 and 3 on the Fig. 9, first one can see the highest aerodynamic load of the rotor blade as compared to the others IGV/rotor positions. This is the flow without any IGV wake. Moving to the positions 2 to 6, the IGV enters and next, propagates continuously the rotor passage resulting in the significant decrease of the aerodynamic load of the rotor blades, which attains the least value at position 6. This is because the IGV wake is located between the rotor blades causing higher flow disturbances in the blade to blade passage. Moving to positions 5 and 4, the IGV wake moves downstream of the rotor and the aerodynamic load of the rotor blades again grows and attains its maximum at position 4. This change of this flow field can be seen more clearly in Fig. 10, where we can observe the comparison of the circumferential distribution of the relative velocity normalized by U_m inside of the rotor blade channel at different IGV-rotor position, at $Z_r = 0.1$.

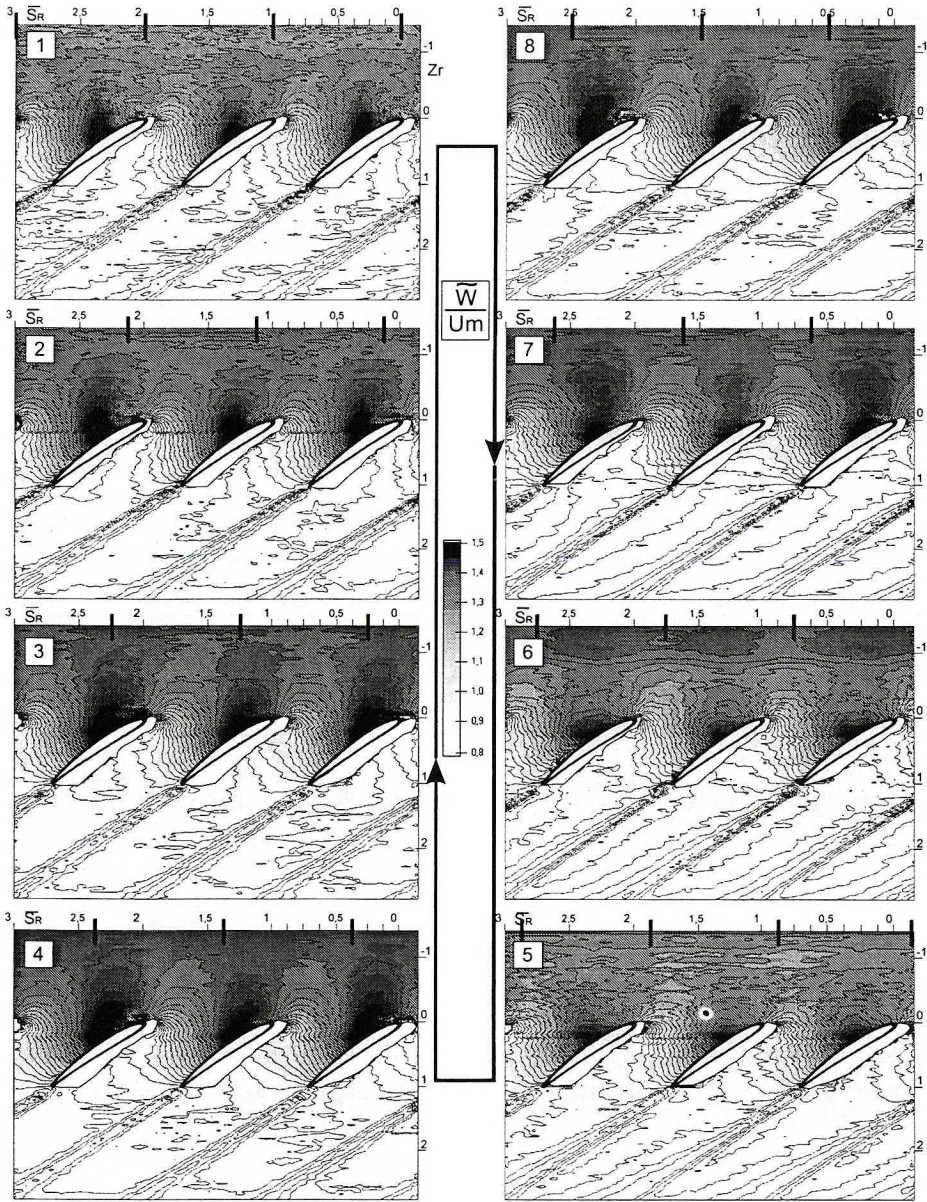


Fig. 9. Contour plots of the relative velocity distribution at the eight IGV/rotor positions $\gamma = -20^\circ$, $\varphi_T = 0.401$, $Y_r = 0.5$, LDA

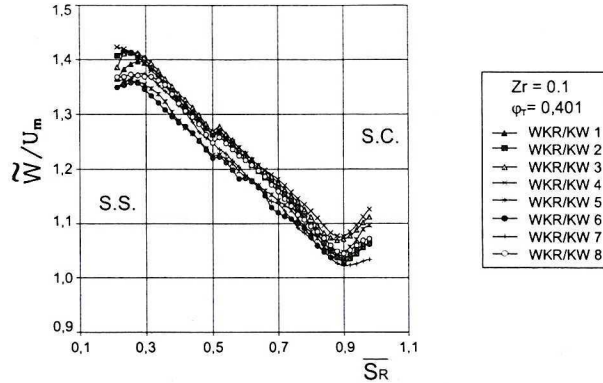


Fig. 10. Variation of the cycle average relative velocity at different IGV-rotor position. $\gamma = -20^\circ$, $Y_r = 0.5$, LDA

The blade-to-blade profiles of the cycle-averaged relative velocity presented in Fig. 10 show that the IGV-rotor positions have a significant effect on the flow field and confirmed earlier observations.

3.2.2. Relative unresolved unsteadiness

Fig. 11 shows contour plots of the relative unresolved unsteadiness at eight different IGV/rotor locations.

Examining position 2, one can first see a region of increased unresolved unsteadiness upstream of the rotor leading edge as compared to the ensemble averaged relative unsteadiness upstream of the rotor presented in the position 4. This is the IGV wake. Moving to the position 8 by the position 1, the IGV wake enters the rotor passage and is subsequently chopped into individual segments by the rotor blades. The individual segments of the IGV wake can now move independently of each other, resulting in a mismatch between segments. The blade-to-blade profiles of the unresolved unsteadiness presented in Fig. 11 show that the rotor leading edge has a significant effect on the flow field. There is also increased unresolved unsteadiness near the pressure surface of the rotor blade just downstream of the point where the IGV wake interacts with the rotor pressure surface. In accordance with Fig. 4, the IGV wake should be completely inside the rotor blade-to-blade passage after six IGV/rotor locations. The maximum interaction between the IGV wakes and blade-to-blade flow field occurs when the IGV wake is directly inside the rotor blade-to-blade passage at position 6, where unresolved unsteadiness attains its maximum values. The minimum interaction occurs at position 4, when the IGV wake is outside of the rotor blade channel. This is confirmed by examining the blade-to-blade distribution of the relative velocity and unresolved unsteadiness on the Fig. 12. The lowest unresolved

unsteadiness occurs at position 3 and 4 due to the absence of the IGV wake inside the blade-to-blade passage. At positions 8, 7, 6 IGV wake has moved toward the rotor blade-to-blade channel. This causes significant increase of the unresolved unsteadiness in all region of the rotor passage.

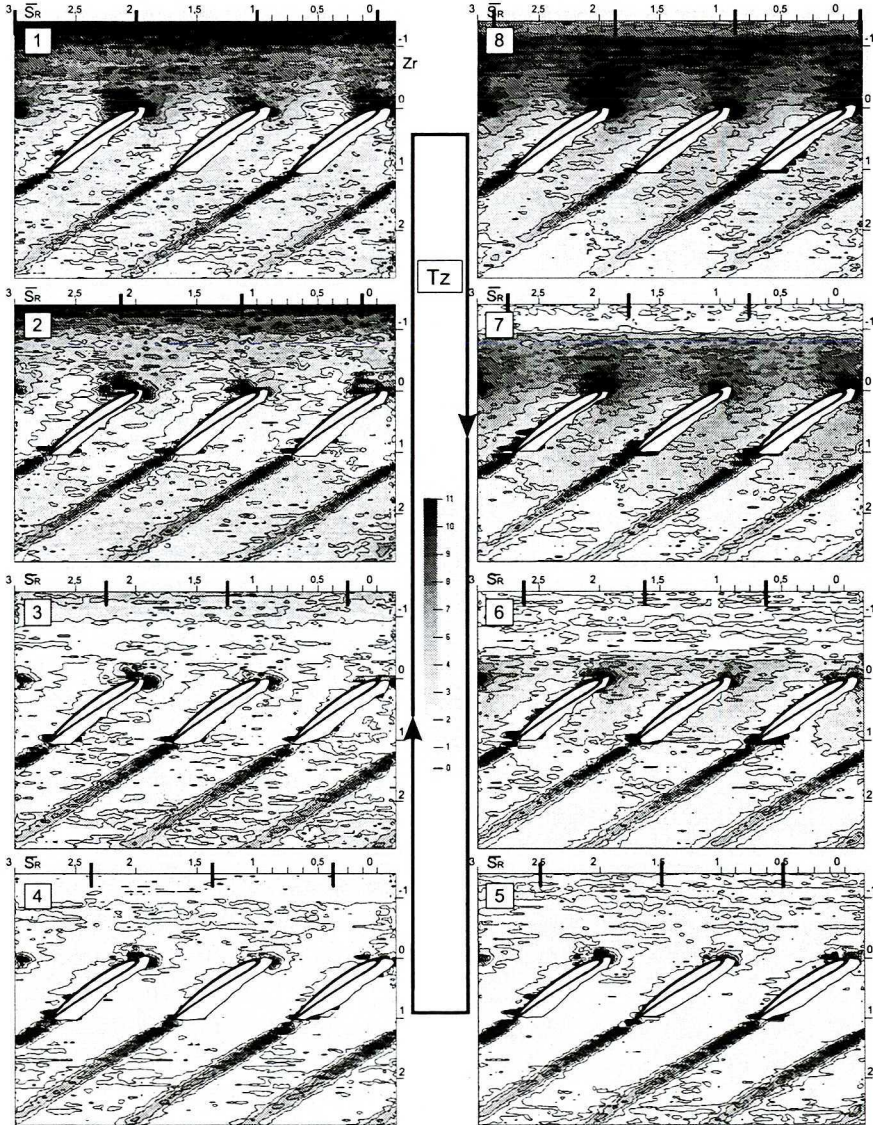


Fig. 11. Axial unresolved unsteadiness at eight IGV/rotor positions at the blade-to-blade rotor passages $\gamma = -20^\circ$, $\varphi_T = 0.401$, $Y_r = 0.5$, LDA

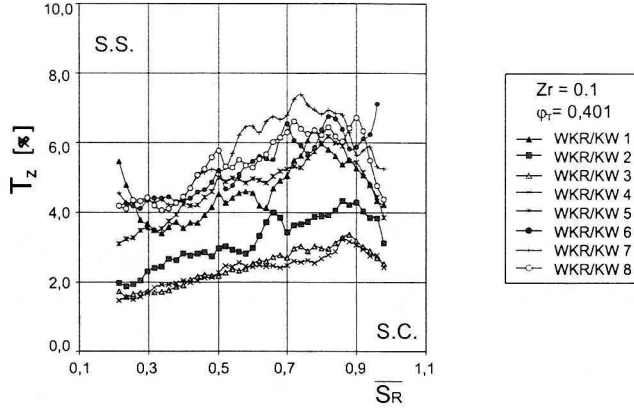


Fig. 12. Rotor axial unresolved unsteadiness circumferential distribution, $\gamma = -20^\circ$, $Y_r = 0.5$, LDA

3.3. Rotor exit flow field

3.3.1. Contour plots of the axial unresolved unsteadiness on the middle radius

The contour plots of the axial unresolved unsteadiness at eight different IVG/rotor locations and at two different IGV stagger angles are presented in Fig. 13 in an absolute frame of reference. Each measurement location is at midspan. They represent eight different instantaneous photographs of the downstream rotor flow field at two different rotor aerodynamic load. It can be seen that the unsteady flow field is not the same at every IGV/rotor position, but changes from one position to another. However, these changes are significantly higher for -20° IGV stagger angle compared to 0° IGV stagger angle. Figure 13 shows also that the rotor blade wake at -20° of the stagger IGV is significantly broader than at 0° stagger angle of IGV. This is due to the higher aerodynamic load of the rotor blade at the higher angle of attack. Figure 13 shows also the highest level of unsteadiness on the suction side of the rotor wake at all IGV/rotor positions, since the suction side surface boundary layer at the blade trailing edge is larger than the pressure surface boundary layer. Measurements of the flow field at 75% axial chord downstream of a rotor, at IGV stagger angle equal -20° with one sensor TSFP, show that there are two distinct flow fields downstream of the rotor, which are called the minimum and maximum interaction between the IGV and rotor wakes. The maximum interaction occurs at position 1 when the IGV wake is directly inside the rotor wake while the region outside the wake shows relatively low total unsteadiness symmetrically on the pressure and suction side of the wake. The minimum interaction occurs at position 5

when the upstream IGV wakes are between the rotor wakes, which is shown by the significant decrease of the level of unsteadiness and slandering of the rotor wake. It can be observed also in Fig. 13 that the maximum level of unsteadiness at the consecutive IGV/rotor positions has moved continuously toward the suction side of the rotor wake. This move increases as the wake travels downstream. Starting from angular IGV/rotor position 6, the wake has moved significantly toward the rotor suction side wake free-stream region.

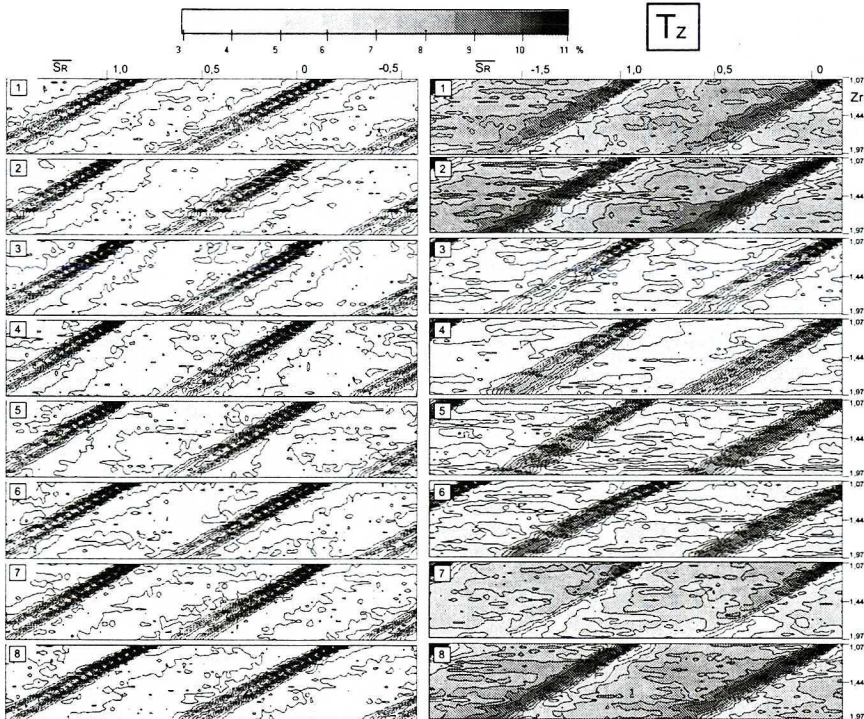


Fig. 13. Axial unresolved unsteadiness at eight IGV/rotor positions and at two stagger angles
a) $\gamma = 0^\circ$, b) $\gamma = -20^\circ$, downstream of the rotor

This causes the suction wake width and free-stream unresolved unsteadiness to increase, since the IGV wake at that IGV/rotor location is located partly in the suction side of the rotor wake and partly in the free-stream region.

3.3.2. Rotor wake profiles at various IGV/rotor passage relative positions

Figures 14 and 15 show the relative velocity profiles and the unresolved unsteadiness in the rotor wake just downstream ($Z_r = 1.97$) of the rotor trailing

edge at all eight IGV/rotor positions and at two stagger angles of the IGV (a) $\gamma = 0^\circ$, b) $\gamma = -20^\circ$). There is a variation in both the velocity profile inside the wake and in the free stream for all eight positions at both stagger angles of the IGV. However, this variation is noticeably higher at -20° of the IGV stagger angle. The highest and most symmetric wake velocity defect, at that stagger angle, occurs at relative IGV/rotor angular position 3 due to the presence of the IGV wake inside the rotor wake at this position. It is consistent with the conclusions drawn earlier. At the relative IGV/rotor angular position 5, the IGV wake has moved toward the rotor wake free-stream region. This causes the suction side wake width to increase and the free stream velocity to decrease, since the IGV wake at that location is located partly in the suction side of the rotor wake and partly in the free stream region. Starting from position 6 and proceeding to the position 8, the wake center velocity increases, while the free-stream velocity decreases due to movement of the IGV wake into the suction side free-stream region at there positions. This is consistent with the conclusions derived earlier and agrees with the results of Zaccaria and Lakshminarayana [3], who measured the flow field in a turbine rotor with a realistic nozzle-rotor spacing; their results include both potential flow and wake interactions. Also, the wake profiles are asymmetric about the wake center due to the differential growth of the boundary layer on the pressure side wake, since the suction surface boundary layer at the blade trailing edge is larger than the pressure surface boundary layer.

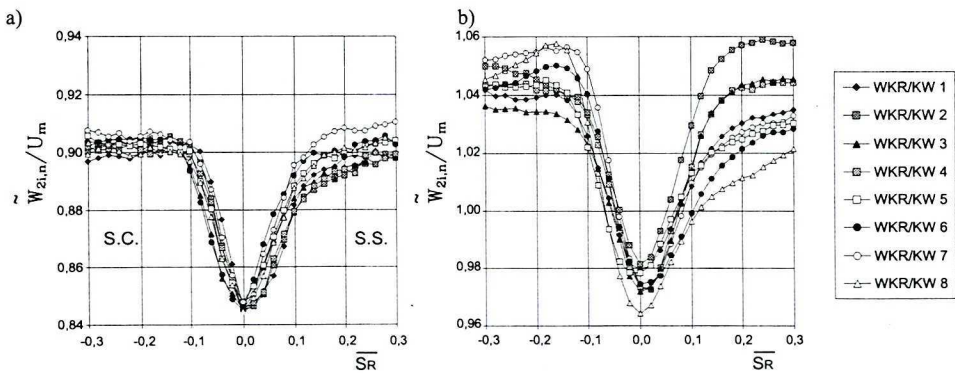


Fig. 14. Rotor wake velocity profiles at $Z_r = 1.97$ and at two stagger angle of IGV
 a) $\gamma = 0^\circ$, b) $\gamma = -20^\circ$

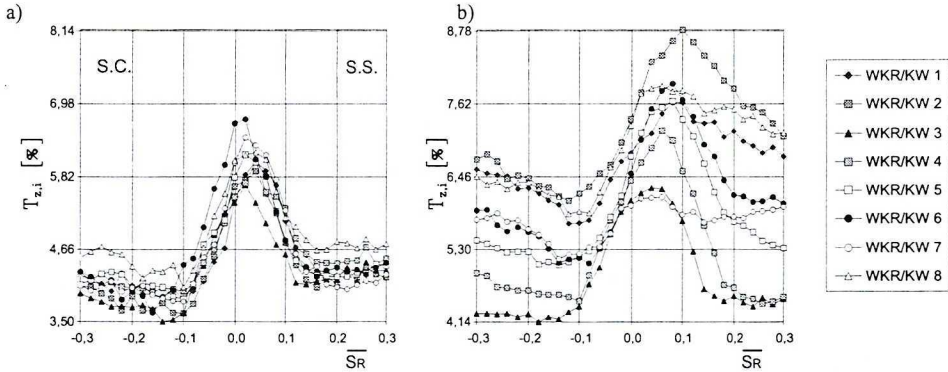


Fig. 15. Rotor wake unresolved unsteadiness at $Z_r = 1.97$ at two stagger angle of IGV
 a) $\gamma = 0^\circ$, b) $\gamma = -20^\circ$

The unresolved unsteadiness at 0° and -20° IGV stagger angles presented in Fig. 15 shows the increased levels of unsteadiness on the suction side of the rotor wake at position 8 due to presence of the IGV wake in this region. At position 5, the level of unsteadiness has decreased in the wake but has relatively increased in the free stream region since the IGV wake is partially in the free-stream region. The IGV wake has moved entirely into the suction side of the free-stream region, as shown by the relatively higher level of unsteadiness in the free-stream region and lower level in pressure side of the rotor wake.

The unresolved unsteadiness increased significantly both in the rotor wake and in the free-stream region at the -20° setting angle of the IGV in comparison with the unresolved unsteadiness at the 0° setting angle of IGV.

3.3.3. The decay characteristics of the rotor wake with streamwise distance

A knowledge of the rate of decay for the rotor wake defect and unresolved unsteadiness is necessary for the understanding the rotor-stator interaction. In order to make the discussion easier, the rotor wake can be classified, according to the work [3], into three different regions: the trailing edge region, near wake region and far wake region.

The decay of the wake velocity defect and maximum unresolved unsteadiness in the rotor wake with streamwise distance is shown in Figures 16 and 17 for each of the IGV/rotor positions at two different stagger angles of the IGV. While the wake velocity defect and maximum unresolved unsteadiness are very high in the trailing edge region, they decay rapidly as the wake travels downstream. The decay rate for each of the IGV/rotor positions is similar, but magnitudes of the velocity defects and unresolved unsteadiness are different

at each streamwise location. This difference is considerably higher at the -20° of the IGV stagger angle, Figures 16b and 17b. Thus, while the IGV wake does not seem to have an impact on the velocity defect decay rate, it does influence the magnitude of the velocity defect, which is significantly stronger at the higher aerodynamic load of the rotor blades. The IGV wake interaction with the rotor wake also affects the rotor wake semi-wake width at two different IGV stagger angles, as shown in Fig. 18.

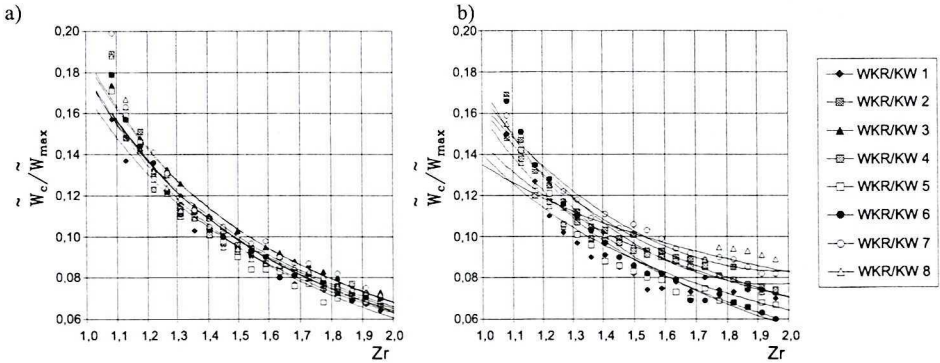


Fig. 16. Decay of rotor wake velocity defect with streamwise distance for each IGV/rotor position at two stagger angles of IGV a) $\gamma = 0^\circ$, b) $\gamma = -20^\circ$

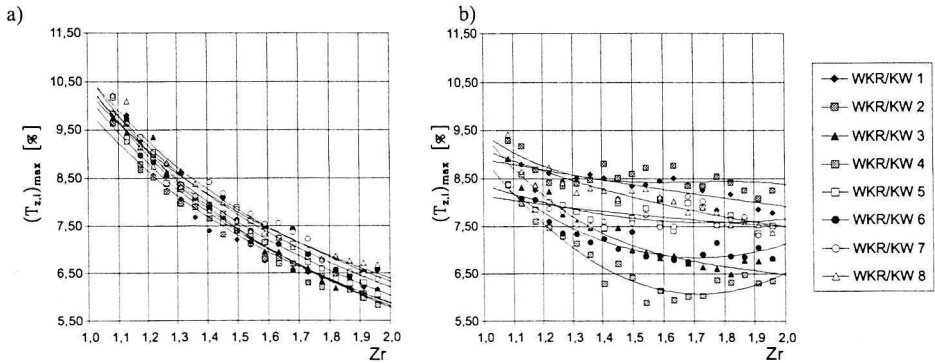


Fig. 17. Decay of maximum unresolved unsteadiness with streamwise distance for each IGV/rotor position at two stagger angles of IGV a) $\gamma = 0^\circ$, b) $\gamma = -20^\circ$

The semi-wake width is defined as the width of the wake at half the defect of total velocity. At the 0° of IGV stagger angle, the rate of increase in wake width for each of the IGV/rotor positions is similar, but the magnitude of the semi-wake width at each streamwise location is not the same for each IGV/rotor location. However, at the -20° stagger angle of the IGV, the rotor

semi-wake width increase much faster at the near and far wake region mainly at the IGV/rotor positions 4 and 5 due to the fact that the IGV wake on in the outer edge between the wake and free stream, which influences the mixing and wake spreading. Thus, just as for the velocity defect, the IGV wake influences the magnitude of the semi-wake width. It is interesting to note that position 5 has the highest rate of increase in wake width. Position 3, consistent with the unresolved unsteadiness, has the lowest wake width of all the wake regions.

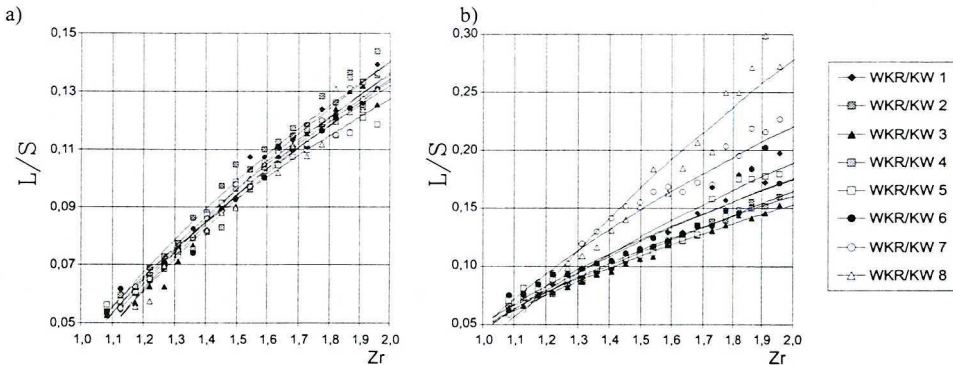


Fig. 18. Variation of rotor wake semi-wake width with streamwise distance at each IGV/rotor position a) $\gamma = 0^\circ$, b) $\gamma = -20^\circ$

3.3.4. Spanwise characteristics of the unsteady flow at different setting angles of IGV

In order to get the spanwise characteristics of the unsteady flow, 38 radial measurements were carried out just downstream of the rotor blade ($Z_r = 1.44$) at 8 IGV/rotor position and at setting angle of IGV $\gamma = -20^\circ$.

While the contour plots of measured velocity distribution in the relative frame are shown in Fig. 19, the contour plots of turbulence intensities are shown in Fig. 20. The wake can be clearly identified by sharp gradients of velocities in the wake region (Fig. 19) and increased turbulent kinematic energy level (Fig. 20). The center of the wake where the unsteady velocities reach their minima are marked by the dotted line. Three major flow features can be seen from these plots, the endwall flow near the hub, the wake along the span, and the influence of the tip leakage near the shroud.

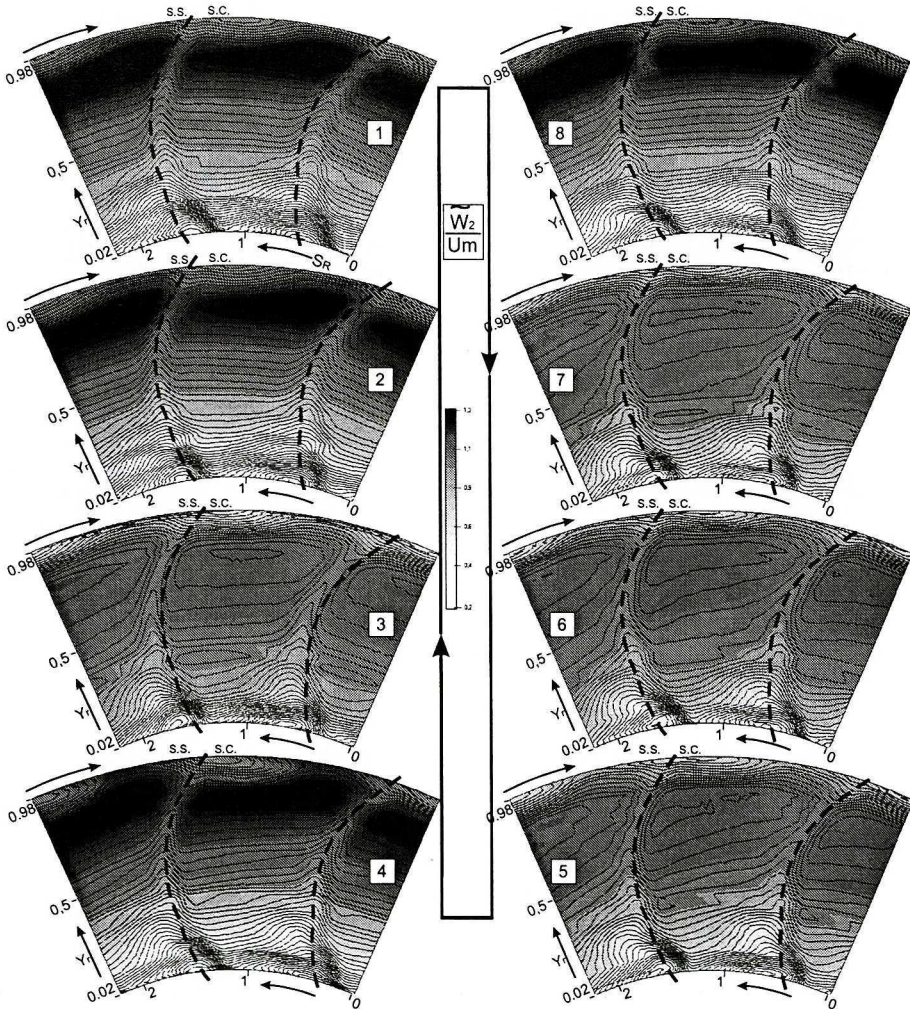


Fig. 19. Relative velocity contour plots downstream of the rotor at $Z_r = 1.44$, $\gamma = -20^\circ$, $\varphi_T = 0.401$, TSFP

It is expected that these three phenomena dominate the generation of unsteadiness downstream of the rotor. For all cases, the turbulent nature of the suction side boundary layer accounts for a thicker wake and higher region of unsteadiness at the suction side, which is significantly more extended at the hub and tip than in the mainstream flow. At the high angle of attack, the rotor blade wake at the hub and at the outer wall becomes wider and the region of unsteadiness increases noticeably. The region of highest instabilities, which occurs at the stagger angle of the IGV -20° on suction side of the wake, indicates the possible appearance of a hub corner separation.

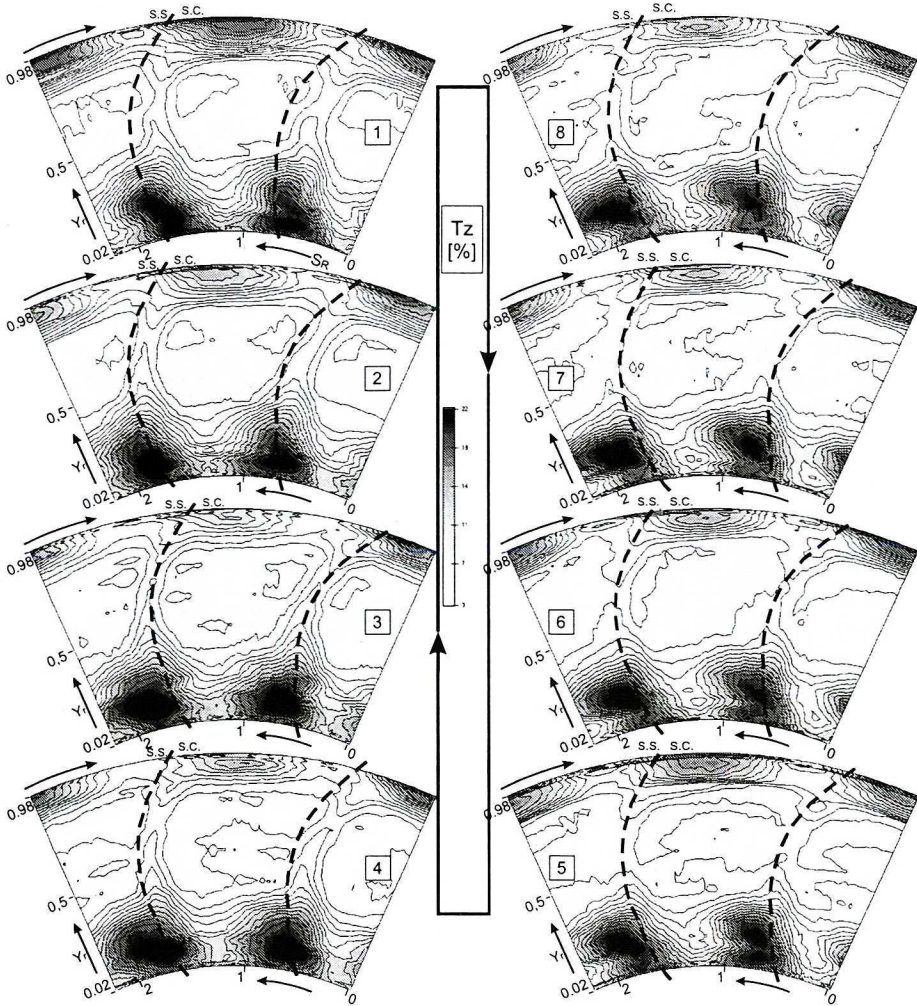


Fig. 20. Axial component of turbulence contour plots downstream of the rotor at $Z_r = 1.44$,
 $\gamma = -20^\circ$, $\varphi_T = 0.401$, TSFP

4. Conclusions

The axial flow low speed compressor stage flow field was measured with a two component LDA inside the rotor and with a two component of TSFP in the IGV-Rotor and Rotor-Back Stator Vanes blade row spacings to gain a better understanding of the unsteady flow due to IGV interaction with the rotor at the different stagger angles of the IGV. These measurements show that the flow field on the rotor leading edge has a major influence on the flow field inside and downstream of the rotor. Changes of compressor load by an

increase of the angle of attack cause significant increase of aerodynamic load and change the unsteady flow field characteristics downstream of the rotor. The highest fluctuations of the velocity, the flow angle and the turbulence intensity are detected in the hub and in the tip region, where leakage flow and three-dimensional effects are dominant. The region of the fluctuation becomes higher as the angle of attack is increased. The region of highest turbulence intensities and turbulence correlations is found close to the hub on the suction side of the blade, with extended corner stall. The movement of the rotor relative to the stator is simulated by changed relative circumferential positions between IGV and rotor. The IGV wake can be easily identified in the rotor passage. The rotor wake is not steady in the rotor time frame, since the rotor wake properties vary between individual IGV/rotor locations. At the positions where the IGV wake is inside the rotor wake, the wake center velocity is lower, the wake velocity defect, the unresolved unsteadiness and semiwake thickness are higher compared to the positions where the IGV is not inside the rotor wake. At the positions where the IGV is located in the free-stream region outside of the rotor wake, the free-stream velocity is lower and the unresolved unsteadiness in the free-stream flow is higher. Higher levels of relative unresolved unsteadiness are also observed near the rotor pressure surface. This increase in unresolved unsteadiness is due to the interaction between the IGV wake and the flow near the pressure surface.

Manuscript received by Editorial Board, July 27, 2005;
final version, January 09, 2006.

REFERENCES

- [1] Poensgen C., Gallus H. E.: Three Dimensional Wake Decay Inside of a Compressor Cascade and its Influence on the Downstream Unsteady Flow Field. Part I – Wake Decay Characteristics in the Flow Passage. Paper of the ASME, 1990, No. 90-GT-21.
- [2] Poensgen C., Gallus H. E.: Three Dimensional Wake Decay Inside of a Compressor Cascade and its Influence on the Downstream Unsteady Flow Field. Part II – Rotor Exit Flow Field. Paper of the ASME, 1990, No. 90-GT-21, pp. 0÷18.
- [3] Zaccaria M. A., Lakshminarayana B.: Unsteady Flow Field Due to Nozzle Wake Interaction with the Rotor in an Axial Flow Turbine. Part II – Rotor Exit Flow Field. ASME, Journal of Turbomachinery, 1997, Vol. 119, pp. 214÷224.
- [4] Zaccaria M. A., Lakshminarayana B.: Unsteady Flow Field Due to Nozzle Wake Interaction with the Rotor in an Axial Flow Turbine. Part I – Rotor Passage Flow Field. ASME, Journal of Turbomachinery, 1997, Vol. 119, pp. 214÷224.
- [5] Freudenreich K. and Fransson T. H.: Application of Three Dimensional Laser-Two-Focus Anemometry to Transonic Turbine Flow: Example of an Isolated Stator. 14th Symposium of Measuring Techniques for Transonic and Supersonic Flow in Cascades and Turbomachines at the University of Limerick. 1998.
- [6] Sharma O. P., Pickett G. F., Ni R. H.: Assessment of Unsteady Flows in Turbines. ASME, Journal of Turbomachinery, 1992, Vol. 114, pp. 79÷90.

- [7] Reinhold N., Bohne A.: Experimental Investigation of Unsteady Flow Phenomena in a Three Stage Axial Compressor, 5th European Conference on Turbomachinery, Praha, Czech Republic, 2003, pp. 209÷219.
- [8] Kazimierski Z.: Płaski przepływ przez osiowy stopień maszyny przepływowej o dowolnych parametrach geometrycznych. *Archiwum Budowy Maszyn*, T. XIII, zeszyt 2, 1966, pp. 213÷232.
- [9] Arnone A., Marconcini M., Scotti Del Greco A.: Numerical Investigation of Three-Dimensional Clocking Effects in a Low Pressure Turbine. *Proc. of ASME Turbo Expo 2003*, June 16-19, 2003, pp. 1÷10.
- [10] Arnone A., Pacciani R.: IGV-Rotor Interaction Analysis in a Transonic Compressor Using the Navier-Stokes Equations. *ASME Journal of Turbomachinery*, 120, No 1, pp. 143÷155.
- [11] Nihuis R., Bohne A., Hoynacki A.: Experimental Investigation of Unsteady Flow Phenomena in a Three Stage Axial Compressor. 5th European Conference on Turbomachinery, Fluid Dynamics and Thermodynamics. Praha, Czech Republic, 2003, pp. 209÷219.
- [12] Witkowski A., Chmielniak T., Stozik M., Majkut M., Żukowski J.: Experimental and Computational Investigations of the Unsteady Flow in an Axial Flow Low Speed Compressor Stage. 6th European Conference on Turbomachinery, Conference Proceedings, Lille, 2005, pp. 168÷177.
- [13] Witkowski A., Chmielniak T., Mirski M., Stozik M.: Stand for Investigations of Three-Dimensional Turbulent Flow in Axial Compressing Stage. *The Archive of Mechanical Engineering*. Vol. XII, 1994, 3–4, pp. 235÷254.
- [14] Witkowski A., Chmielniak T., Stozik M., Mirski M.: Facility for Turbulence and Unsteadiness Measurement Before and Behind an Axial Compressor Rotor Blade by Means of Periodic Multisampling with Triple-Split Fiber Probes. *Proceedings of the 1994 Engineering System Design and Analysis Conference*, Vol. 8, Part B American Society of Mechanical Engineers, New York, 1996, pp. 519÷526.
- [15] Giess P. A., Kost F.: Detailed Experimental Survey of the Transonic Flow Field in a Rotating Annular Turbine Cascade. 2nd European Conference on Turbomachinery, Belgium, 1997.
- [16] Jorgensen F. E.: Characteristics and Calibration of a Triple-Split Probe for Reversing Flows, *DISA Information*, 1982, No. 27.
- [17] Zaccaria M.: An Experimental Investigation into the Steady and Unsteady Flow Field in an Axial Flow Turbine, Ph. D. Thesis, Pennsylvania State University.

Badania eksperymentalne wzajemnego oddziaływania łopatek wlotowej kierownicy regulacyjnej z kołem wirnikowym osiowego niskoobrotowego stopnia sprężającego

Streszczenie

Przeprowadzono badania eksperymentalne dwuwymiarowego ustalonego i nieustalonego pola przepływu, z zastosowaniem dwóch, działających na całkowicie różnej zasadzie, systemów pomiarowych: sondy termoanemometrycznej z trójrozdzielną folią (TSFP) oraz dwuwymiarowego systemu pomiarowego z laserowym anemometrem dopplerowskim (LDA), w celu określenia wzajemnego oddziaływania łopatek wlotowej kierownicy regulacyjnej (IGV) na przepływ w kole wirnikowym. W celu wyznaczenia niejednorodnego pola prędkości na wlocie do koła wirnikowego pomiary prowadzone były w ośmiu położeniach obwodowych, równo rozmieszczonych wzdłuż jednej podziałki łopatek wlotowej kierownicy regulacyjnej. Badania prowadzone w kolejnych krokach czasowych, prowadzone z wykorzystaniem TSFP oraz LDA, umożliwiły określenie pola prędkości, kątów przepływu oraz intensywności turbulencji w różnych wzajemnych położeniach IGV –

koło wirnikowe w czasie przejścia jednej podziałki łopatek. Zmierzone prędkości zostały zdekomponowane do prędkości średniej, składowej periodycznej prędkości oraz składowej prędkości pulsacyjnej. Zastosowanie dwóch systemów pomiarowych, intrusywnego i nieintrusywnego, do pomiaru tego samego skomplikowanego przepływu, umożliwiło przeprowadzenie krytycznego porównania uzyskanych wyników. Uśrednienie uzyskanych wyników umożliwiło również ich porównanie z wynikami pomiarów, przeprowadzonych za pomocą pięciootworowej sondy aerodynamicznej.